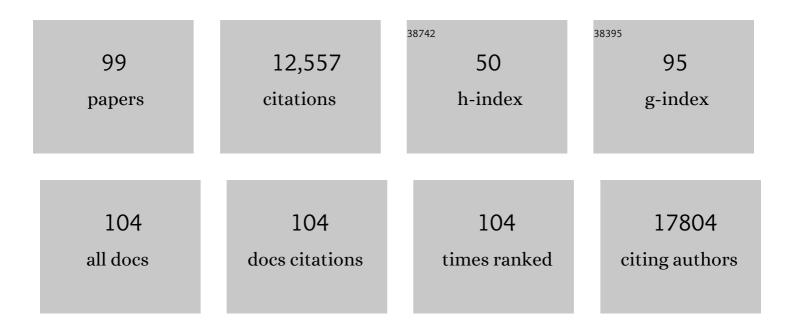


## List of Publications by Year in descending order

Source: https://exaly.com/author-pdf/9253036/publications.pdf Version: 2024-02-01



Vi Vi i

#	Article	IF	CITATIONS
1	Atomically thin two-dimensional organic-inorganic hybrid perovskites. Science, 2015, 349, 1518-1521.	12.6	1,159
2	Synergistic geometric and electronic effects for electrochemical reduction of carbon dioxide using gold–copper bimetallic nanoparticles. Nature Communications, 2014, 5, 4948.	12.8	1,062
3	Atomic structure of sensitive battery materials and interfaces revealed by cryo–electron microscopy. Science, 2017, 358, 506-510.	12.6	1,039
4	Solution-Phase Synthesis of Cesium Lead Halide Perovskite Nanowires. Journal of the American Chemical Society, 2015, 137, 9230-9233.	13.7	861
5	Electrochemical Activation of CO <sub>2</sub> through Atomic Ordering Transformations of AuCu Nanoparticles. Journal of the American Chemical Society, 2017, 139, 8329-8336.	13.7	529
6	MXene (Ti <sub>3</sub> C <sub>2</sub> ) Vacancy-Confined Single-Atom Catalyst for Efficient Functionalization of CO <sub>2</sub> . Journal of the American Chemical Society, 2019, 141, 4086-4093.	13.7	479
7	Synthesis of Composition Tunable and Highly Luminescent Cesium Lead Halide Nanowires through Anion-Exchange Reactions. Journal of the American Chemical Society, 2016, 138, 7236-7239.	13.7	397
8	Bacteria photosensitized by intracellular gold nanoclusters for solar fuel production. Nature Nanotechnology, 2018, 13, 900-905.	31.5	362
9	Growth and Anion Exchange Conversion of CH <sub>3</sub> NH <sub>3</sub> PbX <sub>3</sub> Nanorod Arrays for Light-Emitting Diodes. Nano Letters, 2015, 15, 5519-5524.	9.1	342
10	A Molecular Surface Functionalization Approach to Tuning Nanoparticle Electrocatalysts for Carbon Dioxide Reduction. Journal of the American Chemical Society, 2016, 138, 8120-8125.	13.7	340
11	Molecular engineering of organic–inorganic hybrid perovskites quantum wells. Nature Chemistry, 2019, 11, 1151-1157.	13.6	302
12	Two-dimensional halide perovskite lateral epitaxial heterostructures. Nature, 2020, 580, 614-620.	27.8	284
13	Ultralow thermal conductivity in all-inorganic halide perovskites. Proceedings of the National Academy of Sciences of the United States of America, 2017, 114, 8693-8697.	7.1	246
14	Anisotropic phase segregation and migration of Pt in nanocrystals en route to nanoframe catalysts. Nature Materials, 2016, 15, 1188-1194.	27.5	244
15	Hybrid bioinorganic approach to solar-to-chemical conversion. Proceedings of the National Academy of Sciences of the United States of America, 2015, 112, 11461-11466.	7.1	234
16	Ultrathin Colloidal Cesium Lead Halide Perovskite Nanowires. Journal of the American Chemical Society, 2016, 138, 13155-13158.	13.7	234
17	Stabilization of 4H hexagonal phase in gold nanoribbons. Nature Communications, 2015, 6, 7684.	12.8	215
18	Tandem Catalysis for CO <sub>2</sub> Hydrogenation to C <sub>2</sub> –C <sub>4</sub> Hydrocarbons. Nano Letters, 2017, 17, 3798-3802.	9.1	183

#	Article	IF	CITATIONS
19	Synthesis of Ultrathin Copper Nanowires Using Tris(trimethylsilyl)silane for High-Performance and Low-Haze Transparent Conductors. Nano Letters, 2015, 15, 7610-7615.	9.1	179
20	Control of Architecture in Rhombic Dodecahedral Pt–Ni Nanoframe Electrocatalysts. Journal of the American Chemical Society, 2017, 139, 11678-11681.	13.7	166
21	Solution-Processed Copper/Reduced-Graphene-Oxide Core/Shell Nanowire Transparent Conductors. ACS Nano, 2016, 10, 2600-2606.	14.6	155
22	MOFâ€Confined Subâ€2 nm Atomically Ordered Intermetallic PdZn Nanoparticles as Highâ€Performance Catalysts for Selective Hydrogenation of Acetylene. Advanced Materials, 2018, 30, e1801878.	21.0	133
23	Structural, optical, and electrical properties of phase-controlled cesium lead iodide nanowires. Nano Research, 2017, 10, 1107-1114.	10.4	128
24	Strongly Quantum Confined Colloidal Cesium Tin Iodide Perovskite Nanoplates: Lessons for Reducing Defect Density and Improving Stability. Nano Letters, 2018, 18, 2060-2066.	9.1	128
25	Directed Assembly of Nanoparticle Catalysts on Nanowire Photoelectrodes for Photoelectrochemical CO <sub>2</sub> Reduction. Nano Letters, 2016, 16, 5675-5680.	9.1	125
26	Atomic Resolution Imaging of Halide Perovskites. Nano Letters, 2016, 16, 7530-7535.	9.1	125
27	Ultrathin Epitaxial Cu@Au Core–Shell Nanowires for Stable Transparent Conductors. Journal of the American Chemical Society, 2017, 139, 7348-7354.	13.7	125
28	Core–Shell CdS–Cu <sub>2</sub> S Nanorod Array Solar Cells. Nano Letters, 2015, 15, 4096-4101.	9.1	114
29	Covalent Triazine Framework Confined Copper Catalysts for Selective Electrochemical CO <sub>2</sub> Reduction: Operando Diagnosis of Active Sites. ACS Catalysis, 2020, 10, 4534-4542.	11.2	112
30	General Way To Construct Micro- and Mesoporous Metal–Organic Framework-Based Porous Liquids. Journal of the American Chemical Society, 2019, 141, 19708-19714.	13.7	111
31	Atomic Tuning of Single-Atom Fe–N–C Catalysts with Phosphorus for Robust Electrochemical CO <sub>2</sub> Reduction. Nano Letters, 2022, 22, 1557-1565.	9.1	111
32	Allâ€Solidâ€State Batteries with a Limited Lithium Metal Anode at Room Temperature using a Garnetâ€Based Electrolyte. Advanced Materials, 2021, 33, e2002325.	21.0	99
33	Engineering Lattice Disorder on a Photocatalyst: Photochromic BiOBr Nanosheets Enhance Activation of Aromatic C–H Bonds via Water Oxidation. Journal of the American Chemical Society, 2022, 144, 3386-3397.	13.7	96
34	Highâ€Performance, Low ost, and Denseâ€6tructure Electrodes with High Mass Loading for Lithiumâ€lon Batteries. Advanced Functional Materials, 2019, 29, 1903961.	14.9	93
35	Ruddlesden–Popper Phase in Two-Dimensional Inorganic Halide Perovskites: A Plausible Model and the Supporting Observations. Nano Letters, 2017, 17, 5489-5494.	9.1	90
36	Layer-by-layer anionic diffusion in two-dimensional halide perovskite vertical heterostructures. Nature Nanotechnology, 2021, 16, 584-591.	31.5	88

#	Article	IF	CITATIONS
37	Living materials fabricated via gradient mineralization of light-inducible biofilms. Nature Chemical Biology, 2021, 17, 351-359.	8.0	85
38	Atomic Structure of Ultrathin Gold Nanowires. Nano Letters, 2016, 16, 3078-3084.	9.1	82
39	Insights into the Mechanism of Tandem Alkene Hydroformylation over a Nanostructured Catalyst with Multiple Interfaces. Journal of the American Chemical Society, 2016, 138, 11568-11574.	13.7	82
40	Extrinsic and Dynamic Edge States of Two-Dimensional Lead Halide Perovskites. ACS Nano, 2019, 13, 1635-1644.	14.6	79
41	Stabilized lithium metal anode by an efficient coating for high-performance Li–S batteries. Energy Storage Materials, 2020, 24, 329-335.	18.0	79
42	Phase-Selective Cation-Exchange Chemistry in Sulfide Nanowire Systems. Journal of the American Chemical Society, 2014, 136, 17430-17433.	13.7	78
43	A generalizable method for the construction of MOF@polymer functional composites through surface-initiated atom transfer radical polymerization. Chemical Science, 2019, 10, 1816-1822.	7.4	75
44	Thermal Transport in Silicon Nanowires at High Temperature up to 700 K. Nano Letters, 2016, 16, 4133-4140.	9.1	74
45	Growth and Photoelectrochemical Energy Conversion of Wurtzite Indium Phosphide Nanowire Arrays. ACS Nano, 2016, 10, 5525-5535.	14.6	70
46	Electrocatalytic NiCo <sub>2</sub> O <sub>4</sub> Nanofiber Arrays on Carbon Cloth for Flexible and High-Loading Lithium–Sulfur Batteries. Nano Letters, 2021, 21, 5285-5292.	9.1	64
47	Kinetics-Controlled Super-Assembly of Asymmetric Porous and Hollow Carbon Nanoparticles as Light-Sensitive Smart Nanovehicles. Journal of the American Chemical Society, 2022, 144, 1634-1646.	13.7	64
48	Semiconducting amorphous carbon thin films for transparent conducting electrodes. Carbon, 2014, 76, 64-70.	10.3	62
49	Genetic and biochemical investigations of the role of MamP in redox control of iron biomineralization in <i>Magnetospirillum magneticum</i> . Proceedings of the National Academy of Sciences of the United States of America, 2015, 112, 3904-3909.	7.1	62
50	Spontaneous Delithiation under <i>Operando</i> Condition Triggers Formation of an Amorphous Active Layer in Spinel Cobalt Oxides Electrocatalyst toward Oxygen Evolution. ACS Catalysis, 2019, 9, 7389-7397.	11.2	52
51	Electrical and Optical Tunability in All-Inorganic Halide Perovskite Alloy Nanowires. Nano Letters, 2018, 18, 3538-3542.	9.1	51
52	Pyroelectric nanoplates for reduction of CO2 toÂmethanol driven by temperature-variation. Nature Communications, 2021, 12, 318.	12.8	51
53	Phase-transition–induced p-n junction in single halide perovskite nanowire. Proceedings of the National Academy of Sciences of the United States of America, 2018, 115, 8889-8894.	7.1	48
54	Solution Phase Synthesis of Indium Gallium Phosphide Alloy Nanowires. ACS Nano, 2015, 9, 3951-3960.	14.6	44

#	Article	IF	CITATIONS
55	Niobium Tungsten Oxides for Electrochromic Devices with Long-Term Stability. ACS Nano, 2022, 16, 2621-2628.	14.6	44
56	Synthesis of PtCo3 polyhedral nanoparticles and evolution to Pt3Co nanoframes. Surface Science, 2016, 648, 328-332.	1.9	42
57	Benzoin Radicals as Reducing Agent for Synthesizing Ultrathin Copper Nanowires. Journal of the American Chemical Society, 2017, 139, 3027-3032.	13.7	40
58	Electric-field control of phase separation and memory effect in Pr0.6Ca0.4MnO3/Pb(Mg1/3Nb2/3)0.7Ti0.3O3 heterostructures. Applied Physics Letters, 2011, 98, .	3.3	38
59	Cation/Anion Codoped and Cobalt-Free Li-Rich Layered Cathode for High-Performance Li-Ion Batteries. Nano Letters, 2021, 21, 8370-8377.	9.1	35
60	High-performance overall water splitting based on amorphous iron doped cobalt tungstate <i>via</i> facile co-precipitation. Journal of Materials Chemistry A, 2021, 9, 9753-9760.	10.3	34
61	Strain-Mediated Coexistence of Volatile and Nonvolatile Converse Magnetoelectric Effects in Fe/Pb(Mg <sub>1/3</sub> Nb <sub>2/3</sub> ) <sub>0.7</sub> Ti <sub>0.3</sub> O <sub>3</sub> Heterostructure. ACS Applied Materials & Interfaces, 2017, 9, 20637-20647.	8.0	32
62	Unravelling the room-temperature atomic structure and growth kinetics of lithium metal. Nature Communications, 2020, 11, 5367.	12.8	29
63	Room-Temperature Dynamics of Vanishing Copper Nanoparticles Supported on Silica. Nano Letters, 2017, 17, 2732-2737.	9.1	27
64	Direct aerobic oxidation of monoalcohol and diols to acetals using tandem Ru@MOF catalysts. Nano Research, 2021, 14, 479-485.	10.4	27
65	Highâ€Performance Threeâ€Dimensional Li Anode Scaffold Enabled by Homogeneous Zn Nanoclusters. Small, 2020, 16, e2001257.	10.0	25
66	Superconductivity in Vacuum Annealed Bi <sub>6</sub> O <sub>8</sub> S <sub>5</sub> . Journal of the Physical Society of Japan, 2013, 82, 034718.	1.6	22
67	Morphology-controlled transformation of Cu@Au core-shell nanowires into thermally stable Cu3Au intermetallic nanowires. Nano Research, 2020, 13, 2564-2569.	10.4	22
68	Engineering plasticization resistant gas separation membranes using metal–organic nanocapsules. Chemical Science, 2020, 11, 4687-4694.	7.4	22
69	Manganese vacancy-confined single-atom Ag in cryptomelane nanorods for efficient Wacker oxidation of styrene derivatives. Chemical Science, 2021, 12, 6099-6106.	7.4	22
70	Self-assembled Pt–CoFe layered double hydroxides for efficient alkaline water/seawater splitting by spontaneous redox synthesis. Journal of Power Sources, 2022, 532, 231353.	7.8	20
71	Atomic-scale study of topological vortex-like domain pattern in multiferroic hexagonal manganites. Applied Physics Letters, 2013, 103, 032901.	3.3	19
72	<i>In Situ</i> Growth of Strained Matrix on CsPbI <sub>3</sub> Perovskite Quantum Dots for Balanced Conductivity and Stability. ACS Nano, 2022, 16, 10534-10544.	14.6	16

#	Article	IF	CITATIONS
73	Enhanced Oxygen Evolution Activity of CoO–La <sub>0.7</sub> Sr <sub>0.3</sub> MnO <sub>3â^'δ</sub> Heterostructured Thin Film. ACS Applied Energy Materials, 2020, 3, 7988-7996.	5.1	15
74	Improved Electrochemical Performance of Li-Rich Layered Oxide Cathodes Enabled by a Two-Step Heat Treatment. ACS Applied Materials & Interfaces, 2021, 13, 13281-13288.	8.0	15
75	Pr-Doped LaCoO <sub>3</sub> toward Stable and Efficient Oxygen Evolution Reaction. ACS Applied Energy Materials, 2021, 4, 9057-9065.	5.1	15
76	Understanding the formation of multiply twinned structure in decahedral intermetallic nanoparticles. IUCrJ, 2019, 6, 447-453.	2.2	13
77	Microstructure of Lithium Dendrites Revealed by Room-Temperature Electron Microscopy. Journal of the American Chemical Society, 2022, 144, 4124-4132.	13.7	12
78	High-resolution transmission electron microscopy of beam-sensitive halide perovskites. CheM, 2022, 8, 327-339.	11.7	9
79	Atomic distribution, local structure and cation size effect in o-R1â <sup>~,</sup> xCaxMnO3(R = Dy, Y, and Ho). Journa of Physics Condensed Matter, 2013, 25, 475901.	1.8	6
80	Ambipolar two-dimensional bismuth nanostructures in junction with bismuth oxychloride. Nano Research, 2021, 14, 1103-1109.	10.4	6
81	Synthesis of a Spatially Confined, Highly Durable, and Fully Exposed Pd Cluster Catalyst via Sequential Site-Selective Atomic Layer Deposition. ACS Applied Materials & Interfaces, 2022, 14, 14466-14473.	8.0	6
82	The effects of local strain on the cubic Li7La3Zr2O12(001)/Li(001) interface: A first-principles study. Solid State Ionics, 2021, 360, 115546.	2.7	5
83	Structural Damage of Two-Dimensional Organic–Inorganic Halide Perovskites. Inorganics, 2020, 8, 13.	2.7	5
84	Application of Auger electron spectroscopy in lithium-ion conducting oxide solid electrolytes. Nano Research, 0, , .	10.4	5
85	Microstructure and strain relaxation of orthorhombic TmMnO3 epitaxial thin films. Journal of Crystal Growth, 2012, 338, 280-282.	1.5	4
86	Microstructure of epitaxial YBa2Cu3O7â^'δ thin films grown on Pb(Mg1/3Nb2/3)0.7Ti0.3O3 substrates. Journal of Crystal Growth, 2012, 354, 98-100.	1.5	4
87	Low-Temperature Solution-Phase Growth of Silicon and Silicon-Containing Alloy Nanowires. Journal of Physical Chemistry C, 2016, 120, 20525-20529.	3.1	4
88	<i>In Situ</i> Probing the Kinetics of Gold Nanoparticle Thermal Sintering in Liquids: Implications for Ink-Jet Printing. ACS Applied Nano Materials, 2021, 4, 2538-2546.	5.0	4
89	Circumferential Li metal deposition at high rates enabled by the synergistic effect of a lithiophilic and ionic conductive network. Journal of Materials Chemistry A, 2022, 10, 5391-5401.	10.3	4
90	Calcium-Assisted <i>In Situ</i> Formation of Perovskite Nanocrystals for Luminescent Green and Blue Emitters. ACS Applied Nano Materials, 2021, 4, 14303-14311.	5.0	3

#	Article	IF	CITATIONS
91	Towards atomic-scale electron microscopy characterization of single molecular catalysts. Catalysis Today, 2020, 350, 192-196.	4.4	2
92	Probing the Formation of Lithium Metal in an Inert Atmosphere by Big Data-Driven <i>In Situ</i> Electron Microscopy. ACS Applied Energy Materials, 2021, 4, 7226-7232.	5.1	2
93	Atomic-scale study of nanocatalysts by aberration-corrected electron microscopy. Journal of Physics Condensed Matter, 2020, 32, 413004.	1.8	2
94	Pitfalls in Electrochemical Liquid Cell Transmission Electron Microscopy for Dendrite Observation. Advanced Energy and Sustainability Research, 0, , 2100160.	5.8	2
95	Revealing the spatial and temporal distribution of different chemical states of lithium by EELS analysis using non-negative matrix factorization. Micron, 2022, 154, 103213.	2.2	1
96	In Situ Electron Microscopy Study of the Dynamics of Liquid Flow in Confined Cells. ACS Applied Materials & Interfaces, 0, , .	8.0	1
97	Insight into ultrasensitive and high-stability flocculation-enhanced Raman spectroscopy for the <i>in situ</i> noninvasive probing of cupping effect substances. Analyst, The, 0, , .	3.5	1
98	Microstructural Characterization of La- and Ti-Codoped Multiferroic BiFeO\$_{3}\$ Epitaxial Thin Films. IEEE Transactions on Magnetics, 2011, 47, 3780-3782.	2.1	0
99	Rapid defect characterization: The efficiency of diffraction contrastâ€scanning transmission electron microscopy. Microscopy Research and Technique, 2020, 83, 1604-1609.	2.2	0